Correlation reflectance spectroscopy of heterogeneous silver nanoparticle films upon compression at the air/water interface

2008 J. Phys.: Condens. Matter 20 055228

(http://iopscience.iop.org/0953-8984/20/5/055228)

J. Phys.: Condens. Matter **20** (2008) 055228 (8pp) doi:10.1088/0953-8984/20/5/055228

Correlation reflectance spectroscopy of heterogeneous silver nanoparticle films upon compression at the air/water interface

Gaëlle Martin-Gassin[1], Yara El Harfouch[1], Emmanuel Benichou[1,3], Guillaume Bachelier[1], Isabelle Russier-Antoine[1], Christian Jonin[1], Stéphane Roux[2], Olivier Tillement[2] and Pierre-François Brevet[1]

[1] Laboratoire de Spectrométrie Ionique et Moléculaire, UMR CNRS 5579, Université Claude Bernard Lyon 1, Bâtiment Alfred Kastler, 43 Boulevard du 11 Novembre 1918, 69622 Villeurbanne cedex, France
[2] Laboratoire de Physico-Chimie des Matériaux Luminescents, UMR CNRS 5260, Université Claude Bernard Lyon 1, Bâtiment Claude Louis Berthollet, 43 Boulevard du 11 Novembre 1918, 69622 Villeurbanne cedex, France

E-mail: Emmanuel.Benichou@lasim.univ-lyon1.fr

Received 5 November 2007, in final form 19 December 2007
Published 18 January 2008
Online at stacks.iop.org/JPhysCM/20/055228

Abstract
Alkanethiol passivated silver nanoparticles were spread at an air/water interface to form a single monolayer film. The surface pressure isotherms and the UV–visible absorbance spectra of the film were recorded as a function of compression, whereas the dynamic behaviour was investigated by reflectance correlation spectroscopy. The film is shown to be inhomogeneous, formed by domains of particles separated by large areas of low particle density. Two distinct motions were observed: Brownian diffusion of the domains and their translational flow due to convection. From the characteristic diffusion time of the domains, and using a Stokes–Einstein analysis, the domain size is determined as a function of surface compression. The domains start to form and grow once a fixed average particle density is reached. Above this density threshold, the attractive van der Waals forces between the particles are dominating compared with the repulsion forces due to the alkanethiol chains.

1. Introduction

Metallic nanostructures have attracted wide interest in recent years due to their optical and electrical properties that significantly differ from their bulk material counterparts. This has motivated a lot of studies aimed at finding potential applications in various fields such as photonics, bio-imaging or sensor detection [1]. Various techniques have been proposed to elaborate materials with nanometre scale metallic structures. In a bottom-up approach, the idea is to start the elaboration process from elementary bricks of material and assemble them into larger ensembles in an attempt to form ordered structures. Techniques that have previously been employed include, for instance, the self-assembly of molecules or particles onto substrates [2, 3] or Langmuir–Blodgett thin films [4]. Electric [5] and magnetic [3] as well as linear [6–8] and nonlinear [6, 9–12] optical properties of such metallic nanoparticle assemblies have then been investigated. However, there has been very little work in which the films are studied *in situ* while the particle density is continuously changed. To perform such studies, the only requirement is that the nanoparticles have the ability to form stable monolayers at the air/water interface while retaining their mobility. Amphiphilic materials such as fatty acids or phospholipids are good candidates since they easily form monolayers at the air/water interface. By a careful selection of the stabilizing ligand, this is also true for metallic nanoparticles. Hence, there is widespread interest in investigating these air/water suspended systems

[3] Author to whom any correspondence should be addressed.

in situ in a Langmuir trough. However, in these films the dynamics often yield large fluctuations in the observable owing to the incessant motion of the particles. This motion is often an impediment to such studies at the air/water interface but its study will yield some insight into the physical properties of the film. In order to access these dynamics, different techniques are possible, mainly based on correlation spectroscopy, like fluorescence correlation spectroscopy (FCS). This latter technique is indeed useful for characterizing the film at the interface and in particular to obtain the dynamics of the particle domains upon film compression. The FCS technique is based on the analysis of the fluctuation with time of the fluorescence intensity [13]. In most of the works performed so far in chemical or biological physics, for example [14], fluorescent probe molecules were therefore used. With a total internal reflection (TIR) configuration, interfaces can be accessed [15, 16] and linear [17] and nonlinear regimes [18] have both been observed [19, 20]. However, fluorescent probes are not always available for the experiment envisaged and one has to develop other techniques. For instance x-ray FCS [21] or Raman correlation spectroscopy [22] have been proposed to study the dynamics of metallic particles in solution.

In this work we propose to use the intensity fluctuations of light reflected from a silver nanoparticle film deposited at the air/water interface to access the dynamics of the film. Indeed, such a film is non-fluorescent and FCS cannot be used. The nanoparticles were stabilized by dodecanethiol and the dynamics of the film was extracted by the autocorrelation analysis of the reflected intensity fluctuations.

2. Experimental details

2.1. Nanoparticle synthesis

The alkanethiol capped silver nanoparticles were synthesized using the two-phase arrested growth method described by Brust *et al* [23] and Korgel *et al* [24]. In brief, the metallic salt is first dissolved in pure water and then silver ions are transferred into the organic phase (chloroform) using tetraoctylammonium bromide $(C_8H_{17})_4NBr$ (TOAB) as the phase transfer catalyst. Then, 30 ml of an aqueous silver ions solution containing 0.15 g of $AgNO_3$ was added to the chloroform solution (20 ml) of the phase transfer catalyst (2.23 g of TOAB) and stirred vigorously for 1 h. The organic phase was then collected and 0.16 g of dodecanethiol ($C_{12}H_{25}SH$) was added to the phase. The mixture was stirred for another 15 min. Then an aqueous sodium borohydride solution was added as the reducing solution (0.39 g of $NaBH_4$ in 24 ml of deionized water ($\rho > 18$ MΩ)). The reaction mixture was stirred for 12 h and then washed twice with water. The organic nanocrystal rich phase was collected and poured in 300 ml ethanol. The solution was left at a temperature of −18 °C until precipitation took place. The phase was filtered while being washed with water and ethanol to remove the phase transfer catalyst, excess thiols and reaction by-products. Finally, 50 mg of powder was collected and redispersed in chloroform yielding a concentration of about 1.8×10^{17} particles l^{-1}. This concentration was confirmed from the UV–visible absorbance measurements, knowing the particle size from transmission electron microscopy (TEM) and the corresponding absolute absorption cross section from Mie theory and experimental data [25]. The solution conservation time is about several months even if a deposit is observed with high density solutions a few weeks after the synthesis, the latter being easily redispersed with the addition of chloroform.

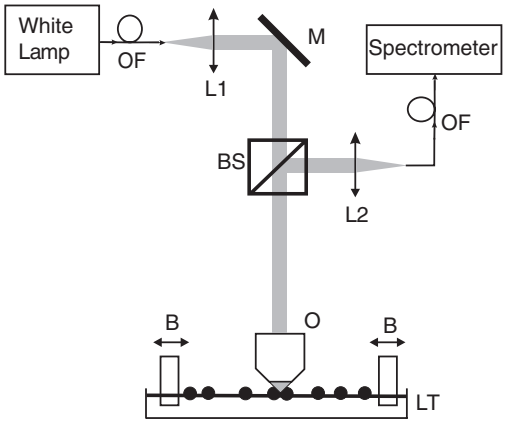

Figure 1. Experimental set-up for measuring the reflected intensity of a silver nanoparticle film upon compression in a Langmuir trough: OF, optical fibre; L, lens; M, mirror; BS, beam splitter; O, objective; Lt, Langmuir trough; B, barrier.

In this synthesis, the length of the alkanethiol chains can be varied from 3 to 18 carbons, thereby varying the minimum inter-particle distance and thus the interaction strength between the particles. Particles coated with long-chain thiols were stable against attractive interactions and had a high hydrophobic character whereas short-chain thiols could undergo much larger inter-particle interactions yielding a lower stability. C_{12} alkyl chains were considered as an intermediate chain length with the minimum edge–edge distance between the particles' metallic cores intermediate between the length of a single C_{12} alkyl chain and that of two chains considering the possible interpenetration of the chains.

Using TEM, the particle size distribution was determined. A drop of the colloidal solution was spread on a carbon-coated copper grid to take the TEM images of the colloids. The images obtained showed that the particles had a rather spherical shape with a diameter of about (8 ± 1) nm.

2.2. Experimental set-up

The experimental set-up is shown in figure 1. Pressure/area isotherms were measured using a Wilhelmy plate in the Langmuir trough (Nima Technology, model 601). All experiments were carried out at room temperature but the liquid phase was held at 15 °C using a variable temperature water circulator inside the PTFE body of the trough to prevent evaporation. All measurements were done with pure water (Millipore water, 18 MΩ cm, pH 7). The trough was thoroughly cleaned before and after each measurement and fresh materials was always used. A 10 μl glass syringe was used to disperse a known amount of particles uniformly

across the water surface. Pressure/area isotherm measurements were carried out using a double barrier compression rate of 6 cm^2 min^{-1}.

The optical measurements were recorded simultaneously with the surface/pressure isotherm. A white light source from a deuterium halogen lamp was coupled to the Langmuir trough through a glass fibre optic. The light exiting the fibre was collimated, passed through a 50/50 beamsplitter and sent at normal incidence on the air/water interface. A microscope objective (×16, NA 0.32) was used to focus the light beam onto the film. The light collected from the film was reflected by the beamsplitter and was collected by another optical fibre at the output of which two different detectors could be connected. The first one, a UV–visible absorbance spectrometer (Ocean Optics, SD2000) was used to obtain a complete spectrum in reflection. These reflection spectra are the result of an averaging procedure over 100 spectra, the integration time of which was 15 ms. The second one, a photomultiplier tube following a monochromator (Jobin Yvon, H10), allowed for a single wavelength measurement with a high sampling frequency. The photomultiplier tube was feeding a correlator to get the autocorrelation function of the intensity signal (Flex02-12D, multiple Tau correlator). The correlator yielded both the intensity as a function of time and the autocorrelation function simultaneously.

3. Results and discussion

3.1. Static UV–visible absorbance

First, static UV–visible absorbance spectra were recorded to give a general view of the surface state. The initial deposit was made of 9×10^{12} particles spread on the 100 cm^2 water surface of the trough. Using this initial surface concentration, the maximum density obtained experimentally at full compression was 4.5×10^{15} particles m^{-2}, whereas the maximum theoretical density for such a film is about 1.6×10^{16} particles m^{-2}. The experimental surface filling factor therefore ranges between about 5% and 30%. For this initial concentration, and at each compression, reflection spectra were recorded. The reflectance of the film was then obtained by dividing the reflection spectra by the reference spectrum obtained from the reflection of the white light on the neat water phase. Figure 2 shows the experimental reflectance versus wavelength for an increasing value of the average surface density for a thiol-capped silver nanoparticle film. The density was increased from 9×10^{14} up to 4.5×10^{15} particles m^{-2} upon surface compression in order to show the manifestation of the inter-particle interactions. The reflectance spectra are normalized to their maximum reflectance value. A reflectance of unity therefore corresponds to a neat air/water interface. When the particles are present at the interface, the reflectance is larger than unity, indicating a reflectance increase. This normalization procedure was done in order to underline the growth of a shoulder between 550 and 750 nm and a red shift of the reflected intensity maximum with compression. These two characteristic features [8, 26] demonstrate the existence of interactions in the nanoparticle film for densities larger than

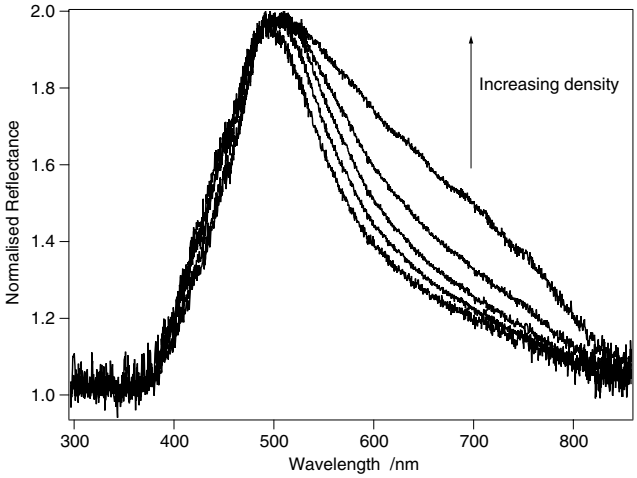

Figure 2. Normalized reflectance versus wavelength for increasing average particle surface densities of a dodecanethiol capped silver nanoparticle film. The average surface nanoparticles densities are, respectively, 1.2, 2.1, 2.6, 3.7 and 4.5×10^{15} particles m^{-2}.

1.2×10^{15} particles m^{-2}. For lower average surface densities, no indication of interaction is observed and therefore all spectra are identical once normalized.

A particularly interesting feature, however, not directly detected in these static UV–visible measurements shown on figure 2 owing to the averaging procedure, is that the reflection signal strongly fluctuates. This phenomenon is especially observed at the lowest densities and diminishes when the film is compressed. These intensity fluctuations dominate at low surface densities owing to film inhomogeneity and the small area spot size. To access the physical parameters driving these fluctuations, the surface was dynamically studied as a function of compression.

3.2. Surface pressure–area isotherms

First, for these low average densities, at average filling factors below 5%, surface pressure–area isotherms were recorded. An initial deposition corresponding to an average particle concentration of 1.7×10^{14} particles m^{-2} and reaching 8.2×10^{14} particles m^{-2} upon compression was spread at the air/water interface. The surface pressure isotherm restricted to this low density surface is presented in figure 3. The isotherm exhibits the characteristics of a classical isotherm for a Langmuir film, although the surface filling factor is rather low compared to that of full monolayer coverage. From 2×10^{14} to 4.5×10^{14} particles m^{-2}, the isotherm does not show any increase in the surface pressure. This suggests that in this regime the nanoparticles are widely dispersed on the subphase without noticeable interactions. From 4.5×10^{14} to 8.2×10^{14} particles m^{-2}, an increase in surface pressure is measured. Interactions between particles take place above a threshold, the value of which can be set at 4.5×10^{14} particles m^{-2}. This value corresponds to a surface filling factor of about 3%. Finally, the surface filling factor reaches a value of 7% at the highest compression, far from the close packed film surface density. The isotherm being an averaged property of the macroscopic

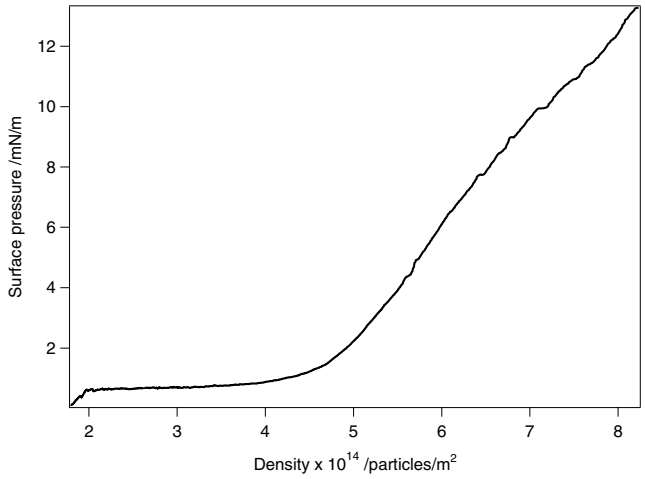

Figure 3. Surface pressure for a dodecanethiol capped silver nanoparticle film surface versus average density.

surface state of the film, the pressure measurements do not show any fluctuations as opposed to the optical measurements made above.

3.3. Intensity fluctuations and correlation function

The intensity fluctuations were recorded as a function of time (see figure 4). Simultaneously isotherms were also measured in order to control the formation of the monolayer. These isotherms are very similar to that presented in figure 3, indicating that the conditions of deposition were identical. The measurements were repeated for six increasing surface densities with a recording time of 120 s. The reflected intensity fluctuations are reported for rather diluted average surface densities, starting from 1.7×10^{14} particles m^{-2} (figure 4 a) and up to 7.5×10^{14} particles m^{-2} (figure 4 f), namely between 1 and 5%. In figure 4(a) at the lowest average density very few sharp peaks are observed above the noise level. Hence for most of the time the reflected intensity is very weak, corresponding to that of the neat air/water interface, with few excursions attributed to the passage of dense particle domains under the objective. It is concluded that the film is therefore rather inhomogeneous even at small average particle densities, where on average the static reflectance barely differs from that of the neat water surface. From figure 4(a) to (f) the peak width and the average reflected intensity increase. In figure 4(f) at the maximum surface density, the intensity is large and constant without fluctuations. These fluctuations can be analysed quantitatively by looking at the autocorrelation function.

The theory used to extract the characteristic times of the surface phenomena using autocorrelation analysis is rather similar to that introduced for fluorescence correlation spectroscopy. At low particle densities, the film may be assumed to be made of two components: domains with a total area S_W of free water surface and domains covered by nanoparticles. If it is assumed that all particle domains have identical areas s_D, only the number of domains N_D will change as a function of time under the light spot. The total area covered by nanoparticle domains is hence the product $N_D \times s_D$. This is a clear oversimplification since the area of the domains must follow a distribution. However, the validity of this approximation leads to an effective number of domains N_D rather than a true number of domains. The light spot area S_{spot} probed by the optical beam therefore writes, with explicit time dependences

$$S_{spot} = S_W(t) + N_D(t)s_D. \tag{1}$$

The observable monitored during the experiment is the power of the reflected light, namely the integral of the reflected intensity over the beam spot at the interface. Hence, it yields:

$$P(t) = \int_{S_{spot}} I_R(t, \vec{r})\, d\vec{r}. \tag{2}$$

In this expression, $I_R(t, \vec{r})$ is the reflected intensity at time t and position $\vec{r}$ within the light spot. This intensity is given by

$$I_R(t, \vec{r}) = \left(R_W + (R_D - R_W)\frac{N_D(t, \vec{r})s_D}{S_{spot}} \right) I_{inc}(\vec{r}) \tag{3}$$

where the two reflectivities R_D and R_W are assumed constant and are, respectively, that of a nanoparticle domain and that of neat water, $I_{inc}(\vec{r})$ is the incident intensity assumed constant over the time without fluctuations. It is therefore assumed that times associated with these fluctuations are much smaller than the times of interest here, as checked by direct control of the fluctuations of the light source. The light beam at the focus has a spatial profile determined from Gaussian optics. Therefore, the incident intensity is given by

$$I_{inc}(\vec{r}) = I_0 \Omega_S(\vec{r}) \tag{4}$$

where I_0 is the maximum intensity collected at the centre of the focus, in the plane of the interface. The expression of the distribution $\Omega_S(\vec{r})$ is given by $\Omega_S(\vec{r}) = \exp(-2(x^2 + y^2)/w_0^2)$ in the plane of the surface [27] where w_0 is the beam waist at the water surface. The value of the parameter w_0 in this experimental set-up is evaluated to about 10 μm. The light spot area S_{spot} is related to the beam waist through the following expression:

$$S_{spot} = \frac{(\int_{S_{spot}} \Omega_S(\vec{r})\, d\vec{r})^2}{\int_{S_{spot}} \Omega_S^2(\vec{r})\, d\vec{r}} = \pi w_0^2. \tag{5}$$

The normalized autocorrelation function $G(\tau)$ of the power $P(t)$ of the reflected beam is hence given as follows:

$$G(\tau) = \frac{\langle P(t+\tau)P(t)\rangle}{\langle P(t)\rangle^2} = 1 + \frac{\langle \delta P(t+\tau)\delta P(t)\rangle}{\langle P(t)\rangle^2} \tag{6}$$

where $\delta P(t)$ is the fluctuation of the collected reflected power. Using equations (2)–(4), it yields

$$\delta P(t) = (R_D - R_W)\frac{s_D}{S_{spot}} I_0 \int_{S_{spot}} \Omega_S(\vec{r})\delta N_D(t, \vec{r})\, d\vec{r}. \tag{7}$$

Two main motions are assumed to drive the surface dynamics at the interface in the time frame accessed during the experiment: the free Brownian diffusion of the particle

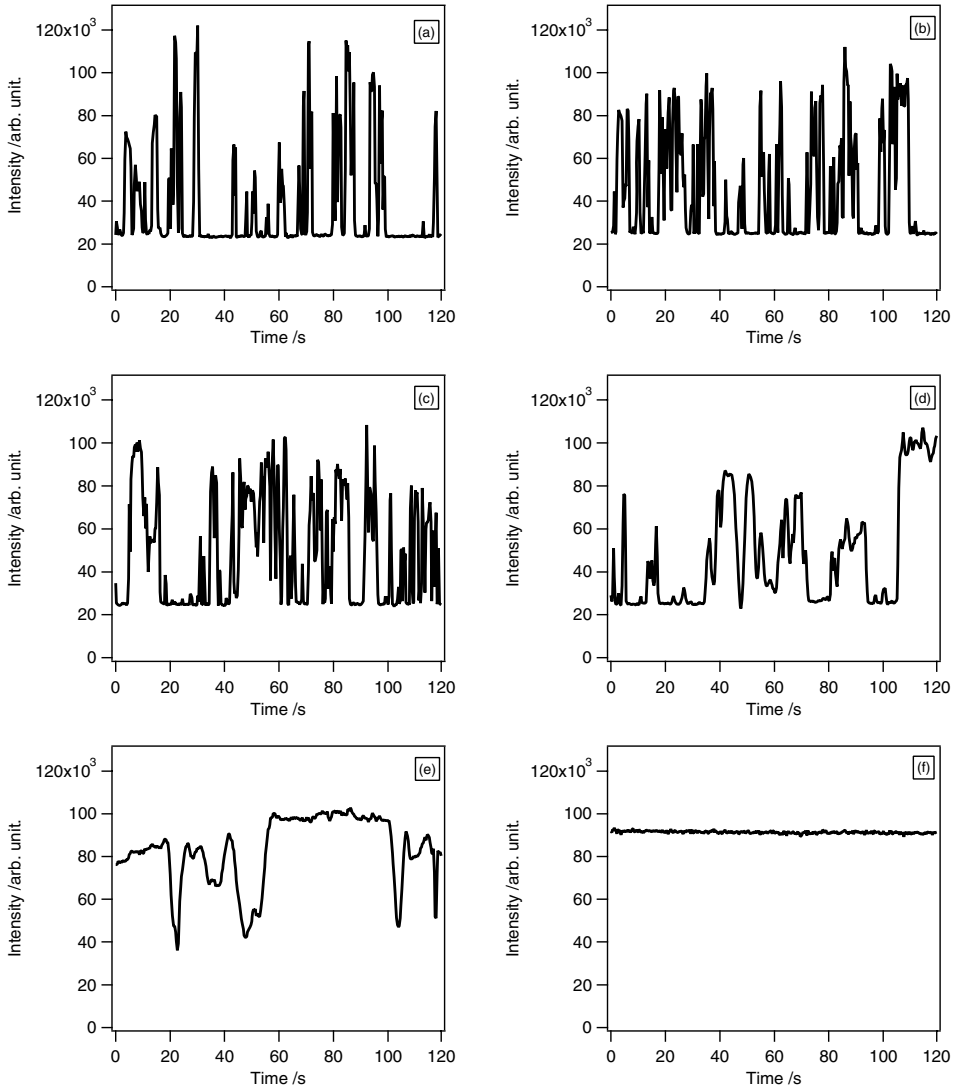

Figure 4. Reflected intensity versus time for a dodecanethiol capped silver nanoparticle film at the air/water interface. The average surface nanoparticle densities are, respectively, (a) 1.8, (b) 3, (c) 3.7, (d) 4.3, (e) 5, (f) 7.5×10^{14} particles m^{-2}.

domains and a uniform surface flow arising from convection. Whereas the assumption about a Brownian random motion of the nanoparticle domains seems natural, the incorporation of the uniform translational motion of the particle domains arising from convection is required in order to fully explain the data. All other sources of fluctuation, like capillary waves or fluid instabilities, were ruled out with blank experiments for the timeframe accessed by the experiment. With domains having the same translational diffusion coefficient, and observing that the flow is only directed in one unique direction defined as y with a uniform velocity v_y, the expression of the correlation function $G(\tau)$ can be determined. This expression has been established by Madge *et al* [28, 29] to describe fluctuations in FCS signals due to a combination of a Brownian diffusion motion and a uniform translation flow. Using their formalism, the expression of the correlation function for the reflected power fluctuations is given by

$$G(\tau) = 1 + \frac{1}{A\langle N_{\mathrm{D}}\rangle}\frac{1}{1+\frac{\tau}{\tau_{\mathrm{D}}}}\mathrm{e}^{\left[-\left(\frac{\tau}{\tau_{\mathrm{f}}}\right)^2\frac{1}{1+\frac{\tau}{\tau_{\mathrm{D}}}}\right]} \tag{8}$$

where A depends on the initial values of the reflectance R_{D} and R_{W}, the area s_{D} and S_{spot} and the average number of domains $\langle N_{\mathrm{D}}\rangle$ under the beam spot through the following relation:

$$A = \left(\frac{R_{\mathrm{W}} S_{\mathrm{spot}}}{(R_{\mathrm{D}} - R_{\mathrm{W}})\langle N_{\mathrm{D}}\rangle s_{\mathrm{D}}} + 1\right)^2. \tag{9}$$

In the case of a dark field experiment like fluorescence spectroscopy, the parameter A is equal to 1 and the expression established by Madge *et al* is retrieved. In our study, this quantity A is very close to unity owing to the weak water reflectivity.

The two other parameters introduced in equation (8) are the free Brownian diffusion time τ_{D} and the uniform flow time τ_{f}. The free Brownian diffusion motion of the domains in an infinite two-dimensional space is defined by the diffusion characteristic time $\tau_{\mathrm{D}} = w_0^2/4D$ where the Stoke–Einstein diffusion coefficient of a domain $D = k_{\mathrm{B}}T/4\pi\eta R$ has been introduced. In this expression, η is the viscosity of the medium, R the dimension of the domain, k_{B} the Boltzmann constant

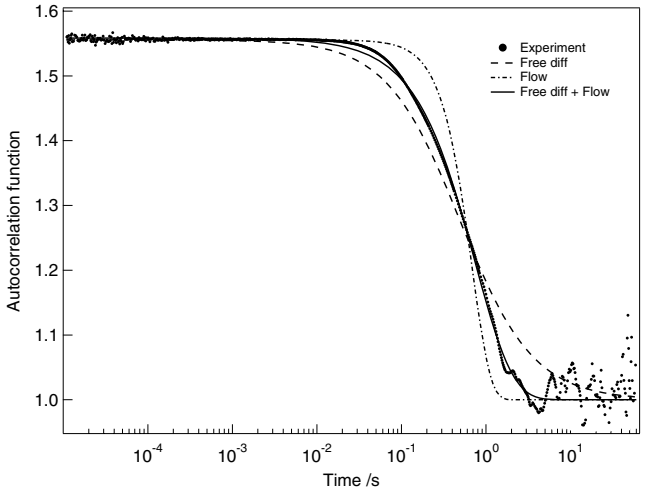

Figure 5. Reflected autocorrelation function calculated from the intensity fluctuations of figure 3(a) for a dodecanethiol capped silver nanoparticle film at the air/water interface. The solid black curve is a fit using equation (8) for a combined uniform flow and diffusion motion; the dashed curve is for free diffusion only and the dotted curve for uniform flow only.

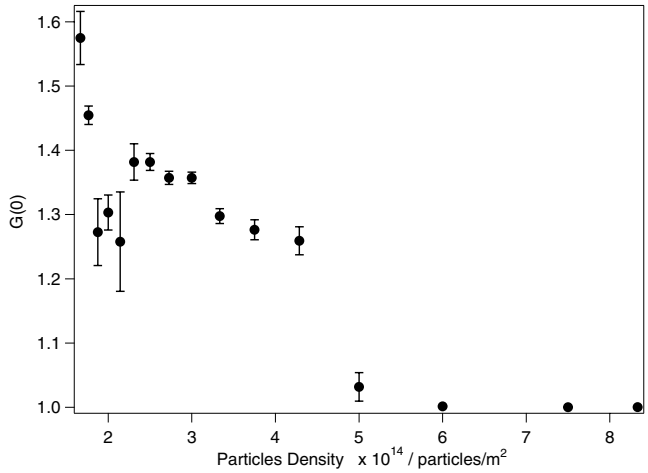

Figure 6. $G(0)$ versus average surface density for a dodecanethiol capped silver nanoparticle film at the air/water interface.

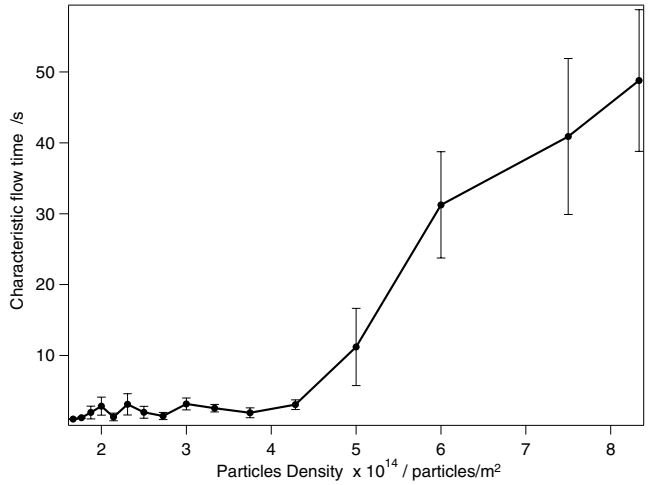

Figure 7. Characteristic flow time versus average surface density for a dodecanethiol capped silver nanoparticle film at the air/water interface.

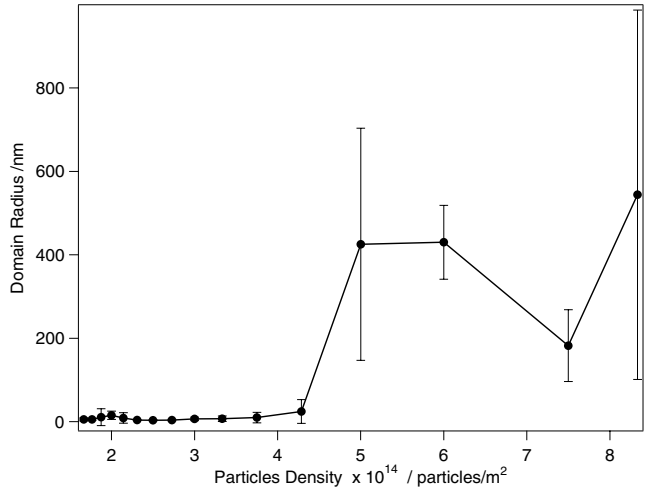

Figure 8. Mean domain radius versus average surface density for a dodecanethiol capped silver nanoparticle film at the air/water interface.

and T the temperature. In addition to this diffusion motion, the uniform flow is defined by its characteristic flow time $\tau_D = w_0^2/v_y$.

3.4. Correlation function as a function of compression

Figure 5 shows the experimental autocorrelation function as a function of delay τ corresponding to the reflected intensity given in figure 4(a). The nanoparticle average density in this case is 1.7×10^{14} particles m^{-2}. Neither the free Brownian diffusion motion alone nor the uniform flow alone can correctly account for the data. It is therefore necessary to introduce the two motions simultaneously using equation (8). In that case, the correlation function given in equation (8) is adequate to account for the data. At later times, re-correlation may occur owing to the successive diffusion of the domains under the light spot. From a fitting procedure, it is then possible to extract the three parameters $A\langle N_D\rangle$, τ_D and τ_f. For each surface compression, the experiments were reproduced five times and the results averaged, yielding a standard deviation. Several compressions with average densities ranging from 1.7×10^{14} to 8.2×10^{14} particles m^{-2} were investigated. The results of this analysis are presented in figures 6–8.

To extract the parameter $A\langle N_D\rangle$, the value of the correlation function $G(\tau)$ at the time origin was used. The average $G(0)$ value is plotted versus the average surface nanoparticle density in figure 6. The theoretical value of $G(0)$ is given by

$$G(0) = 1 + \frac{1}{A\langle N_D\rangle}. \tag{10}$$

Experimentally, $G(0)$ roughly exhibits the expected inverse dependence with the mean number of domains. Indeed, it is expected that as the compression is increased, the

area underneath the beam spot at the interface covered with nanoparticle domains increases. $G(0)$ is, however, not exactly an inverse function of $\langle N_D \rangle$. Indeed, the typical setback observed at a density of 2×10^{14} particles m^{-2} is assumed to arise from the inhomogeneous surface dynamics itself [30]. This interpretation is further supported by the wide error bars reported at these low surface densities. At an approximate average density of 5×10^{14} particles m^{-2}, $G(0)$ reaches a rather constant value close to unity, indicating a rather constant but large value of $\langle N_D \rangle$ according to equation (8). It is interesting to relate this behaviour to that observed on the isotherm in figure 3. Whereas the quantity $\langle N_D \rangle$ remains rather constant, the surface pressure increases regularly. The surface filling coverage is still low, about 3% of the compact layer at this average density of 5×10^{14} particles m^{-2}. Above this threshold, the reflectance is more regular too (see figure 4) indicating the presence of a rather homogeneous film. In this regime of compression, the film is rather dense and the light spot is almost entirely covered by particle domains.

The characteristic flow time extracted from the fitted autocorrelation curves is plotted against the average surface density in figure 7. Its initial value is short, close to 1 s, until the average surface density reaches 4.5×10^{14} particles m^{-2}. Below this average density threshold, the flow is unhindered and the nanoparticle domains move without any stumbling block at an evaluated velocity of a few hundred $\mu m\ s^{-1}$. Above this density threshold, the flow time increases regularly, corresponding to a reduction of the velocity v_y, the domain velocity on the surface. The uniform translation of the nanoparticle domains owing to convection is therefore progressively decelerated. This can be easily understood since the surface gets obstructed as the domains come into close contact and their motion is gradually frozen. Using equation (8), the characteristic diffusion time can also be extracted. With the Stoke–Einstein expression for the diffusion coefficient, an average nanoparticle domain radius is evaluated. These radii are plotted in figure 8 as a function of the average particle surface density. Initially, these radii are rather small, with values of roughly a few nanometres, indicating that the domains at the surface are constituted by a handful of particles at most. Above the threshold average density value, the domain radius rises abruptly, confirming the change of regime from that of dispersed small nanometre scale objects to that of larger aggregated nanoparticle domains. The average domain size reaches values of up to several hundred nanometres.

It appears therefore that, simultaneously with the recording of the static reflectance and the surface–pressure isotherm, the fluctuations of the reflected intensity allow one to get an accurate picture of the film during the compression, and in particular its inhomogeneity. One of the most important observations made is the existence of a common threshold at about 4.5×10^{14} particles m^{-2}, corresponding to a 3% average filling factor. This value is largely below the percolation threshold of the film, which is about 25–30% depending on the initial conditions of aggregation. This low threshold value of 3% is principally determined by the equilibrium between the attractive and the repulsive forces operating between the metallic nanoparticles. The film organization is mainly entropy driven and the two characteristic lengths involved, namely the nanoparticle diameter and the ligand chain length, play an important role in deciding the nature of the organization [31]. The problem cannot be treated as one of hard sphere organization. Based on a study of the effect of the solvent polarity on the self-assembly of ligated metal nanoparticles, Korgel *et al* [24, 32] proposed a soft sphere model taking the particle interaction into consideration where the capped nanoparticles allow for penetration of the ligand shell up the hard sphere limit. In this model the potential energy is considered to be the result of competition between the van der Waals and steric energy [33, 34]. When the attractive force exceeds the repulsive one, a large aggregation of the particles is observed, whereas if the repulsive forces dominate, the film may be more homogeneous with rather small domains. It appears therefore that the combined use of absorbance spectroscopy and pressure–area isotherms with correlation reflectance spectroscopy allows a quantitative study of the film despite large fluctuations in the observables. In the present study, it is observed that an average density threshold exists close to a value of 3% in terms of the average filling factor, determining the equilibrium between the inter-particle forces in the film.

4. Conclusions

A hydrophobic film of thiol-coated silver metallic nanoparticles was spread at the air/water interface and has been studied as a function of simultaneous compression by static and dynamic techniques. In particular, the dynamic studies performed by correlation reflectance spectroscopy reveal the inhomogeneous nature of the film, a picture more difficult to access with averaging techniques like absorbance spectroscopy and pressure–area isotherms. The dynamics of the films is dominated by two processes: a uniform translational flow and a random Brownian diffusion motion. These two motions are modified during the compression, the mobility of the nanoparticle domains tending to slow down when the average density is increased. In the meantime, particle domains of increasing size are formed. The structure of the film is characterized by an average density threshold of about 3% defining two regimes. Below the threshold, at sufficiently large inter-particle distances, the repulsive forces dominate over attractive forces and the size of the domain remains rather small, of the size of a handful of nanoparticles, whereas above the threshold attractive forces dominate and large particle domains are formed.

References

[1] Daniel M C and Astruc D 2004 *Chem. Rev.* **104** 293
[2] Kiely C J, Fink J, Brust M, Bethell D and Schiffrin D J 1998 *Nature* **396** 444
[3] Pileni M P 2001 *J. Phys. Chem.* B **105** 3358
[4] Sastry M, Gole A and Patil V 2001 *Thin Solid Films* **384** 125
[5] Sampaio J F, Beverly K C and Heath J R 2001 *J. Phys. Chem.* B **105** 8797
[6] Remacle F, Collier C P, Markovich G, Heath J R, Banin U and Levine R D 1998 *J. Phys. Chem.* B **102** 7727
[7] Schmitt J, Machtle P, Eck D, Mohwald H and Helm C A 1999 *Langmuir* **15** 3256

[8] Ung T, Liz-Marzan L M and Mulvaney P 2001 *J. Phys. Chem.* B **105** 3441
[9] Collier C P, Saykally R J, Shiang J J, Henrichs S E and Heath J R 1997 *Science* **277** 1978
[10] Galletto P, Girault H H, Gomis-Bas C, Schiffrin D J, Antoine R, Broyer M and Brevet P F 2007 *J. Phys.: Condens. Matter* **19** 375108
[11] Antoine R, Pellarin M, Palpant B, Broyer M, Prevel B, Galletto P, Brevet P F and Girault H H 1998 *J. Appl. Phys.* **84** 4532
[12] Galletto P, Brevet P F, Girault H H, Antoine R and Broyer M 1999 *J. Phys. Chem.* B **103** 8706
[13] Krichevsky O and Bonnet G 2002 *Rep. Prog. Phys.* **65** 251
[14] Hess S T, Huang S H, Heikal A A and Webb W W 2002 *Biochemistry* **41** 697
[15] Lieto A M, Cush R C and Thompson N L 2003 *Biophys. J.* **85** 3294
[16] Hashimoto F, Tsukahara S and Watarai H 2003 *Langmuir* **19** 4197
[17] Hosokawa C, Yoshikawa H and Masuhara H 2005 *Phys. Rev.* E **72** 021408
[18] Berland K M, So P T C, Chen Y, Mantulin W W and Gratton E 1996 *Biophys. J.* **71** 410
[19] Zhao X L, Subrahmanyan S and Eisenthal K B 1991 *Phys. Rev. Lett.* **67** 2025
[20] Zhao X L, Goh M C, Subrahmanyan S and Eisenthal K B 1990 *J. Phys. Chem.* **94** 3370
[21] Wang J, Sood A K, Satyam P V, Feng Y P, Wu X Z, Cai Z H, Yun W B and Sinha S K 1998 *Phys. Rev. Lett.* **80** 1110
[22] Schrof W, Klingler J F, Rozouvan S and Horn D 1998 *Phys. Rev.* E **57** R2523
[23] Brust M, Walker M, Bethell D, Schiffrin D J and Whyman R 1994 *J. Chem. Soc. Chem. Commun.* 801
[24] Korgel B A, Fullam S, Connolly S and Fitzmaurice D 1998 *J. Phys. Chem.* B **102** 8379
[25] Muskens O, Christofilos D, DelFatti N and Vallée F 2006 *J. Opt. A: Pure Appl. Opt.* **8** 264
[26] Wormeester H, Henry A I, Kooij E S, Poelsema B and Pileni M P 2006 *J. Chem. Phys.* **124** 204713
[27] Petrasek Z, Krishnan M, Monch I and Schwille P 2007 *Microsc. Res. Tech.* **70** 459
[28] Elson E L and Magde D 1974 *Biopolymers* **13** 1
[29] Magde D, Webb W W and Elson E L 1978 *Biopolymers* **17** 361
[30] Sear R P, Chung S W, Markovich G, Gelbart W M and Heath J R 1999 *Phys. Rev.* E **59** R6255
[31] Tay K A and Bresme F 2006 *J. Am. Chem. Soc.* **128** 14166
[32] Korgel B A and Fitzmaurice D 1998 *Phys. Rev. Lett.* **80** 3531
[33] Ohara P C, Leff D V, Heath J R and Gelbart W M 1995 *Phys. Rev. Lett.* **75** 3466
[34] Abid J P, Abid M, Bauer C, Girault H H and Brevet P F 2007 *J. Phys. Chem.* C **111** 8849